RESEARCH ARTICLE **ISSN 2738-9898 (Print) ISSN 2738-9901 (Online)**

Assessment and Selection of CMIP6 Climate Models: Application to the Budhigandaki River Basin (BGRB), Nepal

Shankar Lamichhane [1,2] *

[1]Water Engineering and Management, School of Engineering and Technology, Asian institute of Technology, Pathum Thani, 12120, Thailand

[2]School of Engineering, Faculty of Science and Technology, Pokhara University, Kaski, Nepal

*Author to whom correspondence should be addressed; E-Mail: *ershank2014@gmail.com / st124205@ait.asia*

Received : 07 June 2025; Received in revised form : 26 June 2025; Accepted : 01 July 2025; Published: 04 July 2025

Abstract

The most representative CMIP6 Global Climate Models for predicting future climate conditions in the Budhigandaki River Basin (BGRB) are found using an advanced envelope selection method. For each scenario (SSP2-4.5 and SSP5-8.5), four GCMs that best replicate the basin's historical climate and forecast future changes were selected by combining envelope-based range coverage, historical performance assessment, and climate extreme analysis. EC-Earth3-CC, MIROC6, MPI-ESM1-2-LR, and MRI-ESM2-0, representing the Warm-Wet, Warm-Dry, Cold-Dry, and Cold-Wet extremes for SSP2-4.5. For the corresponding climate conditions, IPSL-CM6A-LR, MRI-ESM2-0, GFDL-ESM4, and INM-CM5-0 under SSP5-8.5. These models were selected because they accurately simulated past climatic trends throughout BGRB. The mean air temperature in the basin is predicted to rise by 2.92°C to 3.22°C under SSP2-4.5 and by 3.66°C to 7.07°C under SSP5-8.5 scenarios by the end of the twenty-first century. Forecasts of precipitation show increment with ranges of 0.08% to 17.55% (SSP2-4.5) and 5.00% to 38.97% (SSP5-8.5). These models were chosen because they accurately simulated past climatic trends throughout BGRB. The BGRG's impact assessments and adaptation planning are firmly based on the explicit identification of these models, which faithfully replicate both mean and extreme climate behaviours.

Keywords

Climate Change, GCMs selection, CMIP6, Budhi Gandaki River Basin

1. Introduction

The average atmospheric conditions in a given area over a given period are referred to as the climate. According to the IPCC [1], climate change is defined as long lasting changes in the global climate that are either directly or indirectly brought about by human activity. The IPCC, estimates that global temperatures have increased by 0.3 to 0.6°C since 1900 and are expected to rise by an additional 1.4 to 5.8°C by 2100. The variation in climate involves the interactions between the atmosphere and other components of the climate system such as land, seas, snow, ice, and hydrological systems. Climate change is typically detected through studies of temperature and precipitation patterns.

Floods and droughts are occurring more frequently and with greater intensity due to the effects of climate change, which include changes in temperature and precipitation patterns. Globally, regionally, and domestically, climate change has been a major challenge and source of concern. There has been a noticeable warming trend in Nepal, especially during the winter months. Recent studies provide robust evidence of elevation-dependent warming trends across Nepal. Karki et al. [2] used data from 46 long-term meteorological stations spanning 1980–2016 and that reported significant increases in annual maximum and minimum temperatures at rates of approximately $0.04\ °C\ yr^{-1}$ and $0.02\ °C\ yr^{-1}$, respectively. These warming trends were most pronounced at higher elevations, particularly during the pre-monsoon and winter seasons. Supporting this, Dhital et al. [3] demonstrated that warming intensifies with altitude, with mountainous regions exhibiting greater temperature increases than lowland areas, underscoring elevation as a critical determinant in the spatial variability of climate change impacts across Nepal.

The increasing amounts of carbon dioxide and other greenhouse gases in the atmosphere are closely linked to this warming trend. Climate change is predicted as a result of rising greenhouse gas concentrations in the atmosphere, which are considered in global circulation models (GCMs). The purpose of this model is to predict future weather patterns. Several assumptions regarding the rates at which greenhouse gases will be released into and removed from the atmosphere are included in the model which are referred to as emissions scenarios in the climate model. Global Circulation Models (GCMs), sometimes referred to as Global Climate Models, are complex numerical simulations based on the Navier-Stokes equations that depict the physical processes that occur within the climate system. A climate model is a useful tool for analyzing historical, current, and projected climate change. The most widely used approach for examining climate change involves analyzing temperature and precipitation data. Many GCMs have been developed as a result of the Coupled Model Intercomparison Project's (CMIP) structure changing from CMIP1 to CMIP6 [4]. The uncertainty and bias in GCMs rise with the number of climate models, limiting their usefulness for impact research. Therefore, a comprehensive evaluation of the performance of the wide range of available GCMs is essential.

The number of GCMs that are currently available for predicting future climate change has significantly increased in recent years. Therefore, selecting the best subset of these models is crucial for evaluating regional impacts reliably; however, this process must deal with inherent uncertainties, time, human, and computational constraints. Significant uncertainty in future climate projections is still unavoidable, even with the large number of GCMs and regional climate models (RCMs) in the CMIP5 and CMIP6 archives and ongoing advancements in their physical representations. In general, the past-performance strategy approach assesses how well climate models replicate recent historical climate trends and current climatic conditions [5], [6]. An additional strategy is the "envelope approach," which selects a set of models from the pool of available models to cover a wide range of estimates for one or more of the variables of interest related to climatology [7], [8], [9], with this method, all potential futures as predicted by all the climate models combined will be covered.

In climate impact studies, climate projections from various models are the primary source of uncertainty, outweighing uncertainties from hydrological model parameters and structural configurations [10], [11].

Thus, selecting representative GCMs for a climate change impact study requires careful consideration. One or more criteria may be used in the selection process, but it is crucial to choose a method that is suitable for the intended use. Different approaches can be used to select representative GCMs (1) predicted variations in the yearly precipitation total and mean air temperature[12],[13] as well as predicted variations in climatic extremes; (2) modelling past climate performance for either the means or the extremes[5],[6],[14]; (3) combining the first two methods to create the advanced envelope-based approach[15],[16] and (4) averaging the results of all available GCM runs. However, there are advantages and disadvantages of the selection strategies that should be considered when making your decision [5] used a past-performance method to choose GCMs based on how well they replicated past climate conditions, but Salman et al. [17] selected the envelope-based method to choose models that cover a wide range of future climate projections. The past-performance strategy has a key drawback in that it ignores future estimates of models. Likewise, climate models are chosen at each climatic extreme in the envelope method solely based on annual means. It ignores how well models can replicate historical and contemporary environments. Models with high and low performance are equally weighted when using the average of included GCM runs, which is the main disadvantage. This study used the advanced envelope method, a three-step procedure that combines the envelope approach and past-performance techniques, to choose the best GCMs in order to overcome the aforementioned limitations. Several studies have already chosen representative CMIP5 climate models for different regions using envelope-based and past-performance approaches. All of the findings and conclusions from the CMIP5 climate projections were applied to the Budhigandaki River Basin. However, the IPCC stated in the Sixth Assessment Report that the most recent estimates from the CMIP6 models provide better projections with increased climate sensitivity in comparison to previous forecasts [1].

The primary objective of this research is to identify representative GCMs and use the model outputs to examine trends in observed precipitation and temperature extreme indices. Selecting appropriate climate models is a multi-step process that is usually determined by how well the models replicate past climate trends or how well they capture the entire spectrum of climatic variable changes predicted by all available models. The study of this research aims to select the CMIP6 GCMs by a combination of two thorough methodologies: the historical past-performance approach [5] and the envelope approach [7], [8], [9] and is referred to as an advance-envelope approach. The selection process of this approach involves three methods: (a) comparing the annual average temperature and total precipitation sums; (b) analyzing changes in climate extremes of daily average temperature and precipitation using the Expert Team on Climate Change Detection and Indices (ETCCDI); and (c) making a final decision based on the model's ability to replicate historical climate conditions. The novelty of this project lies in incorporating GCMs from the newly released CMIP6 climate models, which have not previously been considered in the Budhigandaki River Basin (BGRB). Thus,

selecting GCMs from CMIP6 for different SSP scenarios will enhance the accuracy and reliability of GCM selection for BGRB. Planning for climate change adaptation requires crucial knowledge, which the research provided by predicting the climate of the basin and the associated uncertainties using the chosen GCMs. Policymakers rely on the outcomes of impact studies, which use downscaled climate projections to inform and support the development of effective climate change adaptation strategies.

1.2 Study Area and Data Collection

1.2.1 Study Area

The study area is Situated in the central part of Nepal, between 27˚50' and 29˚00'N latitudes and 84˚30' and 85˚10'E longitudes in Dhading and Gorkha districts. The BGRB features a storage-type hydropower project on the Budhigandaki River, located between the Gorkha and Dhading districts, with a drainage area of approximately 5000 km² (as detailed in Supplementary Table 1). The terrain in this basin is rocky, with an elevation range of 315–8115 m above sea level as in Figure 1. The Mowang Khola from the Ladakh Himal and the Shiar Khola from the Lark Himal are the two main tributaries of the Budhi Gandaki River. The river flows about 120 km south from their confluence before joining the Trishuli River at Benighat. The main tributary of the Budhi Gandaki, the Aankhu Khola River, which originates in Ganesh Himal, joins it approximately 24 km upstream from this confluence on the left bank. The Narayani water system, which drains Central Nepal, includes the Budhigandaki. The Narayani basin is composed of five main tributaries: Seti Gandaki, Budhigandaki, Marsyangdi, Trishuli, and Kali Gandaki River. Smooth and regular slopes formed by actively eroding rivers a process accelerated by the recent uplift of the Himalayas define the more developed landscape of the lower region.

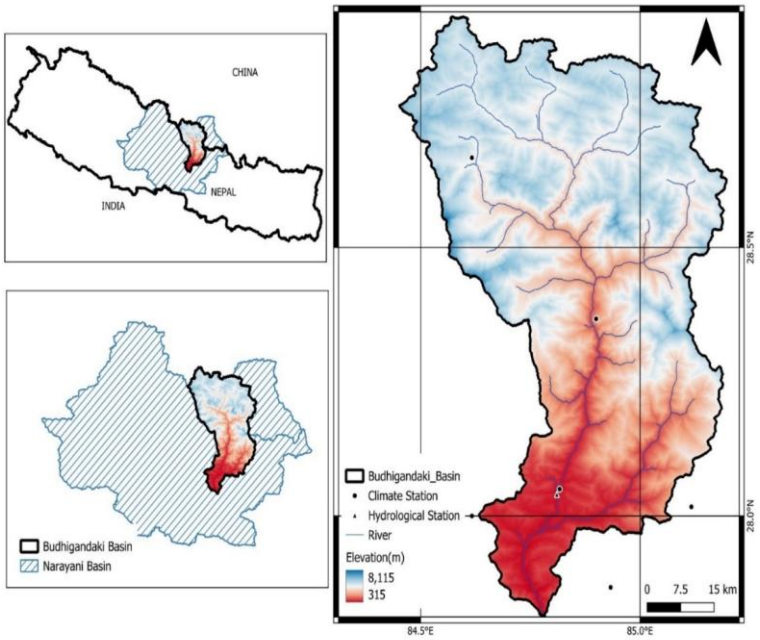

Figure 1: Study Area Budhigandaki River Basin

1.3 Data Collection

1.3.1 Observed Daily Temperature and Precipitation Data

Observed daily precipitation and temperature records were gathered from eight stations to guarantee the accuracy of the historical data. These stations are geographically distributed across the basin to capture the key climatic variability at different elevations and terrains. The meteorological data underwent quality control procedures including consistency checks and, the removal of erroneous records. Nevertheless, some stations exhibited missing data periods, primarily due to equipment maintenance and loss of observation on certain days. To address this, missing data were filled using the arithmetic mean method. The eight stations incorporated in this study are geographically distributed within the BGRB, strategically positioned to capture the region's climatic variability across different elevations and landscape features. The precipitation and temperature data for the period from 1990 to 2014 were sourced from the Department of Hydrology and Meteorology (DHM) and cover both the BGRB and its surrounding areas. The station numbers and their details are shown in Supplementary Table 2. Enhancing spatial coverage with additional observations (e.g., satellite data,) could improve model validation accuracy in such complex terrains for further recommendation.

1.3.2 Climate Models

We first select the GCMs model from the CMIP6 archive (https://cds.climate.copernicus.eu-cmip6), based on daily precipitation, and temperature data for past eras as well as for future scenarios, SSP2-4.5 and SSP5-8.5, with initial conditions of member r1i1p1f1 where 'r' stands for realization index, 'i' for initialization index, 'p' for physics index, and 'f' stands for forcing index. This research used temperature and precipitation projections from all CMIP6 GCMs for two forcing scenarios (SSP2-4.5 and SSP5-8.5), as well as historical data (1970–1999) and future projections (2070–2099). By the end of the twenty-first century, CMIP6 scenarios combine targeted nuclear forcing with the Share Socioeconomic Pathway (SSP). The middle-of-the-road approach combined with reasonable end-of-emission scenarios SSP2-4.5 is based on the SSP-2 with a target radioactive level of 4.5 W/m². Meanwhile, the fossil-fueled development approach combined with a high end-of-emission scenario (SSP5-8.5) is based on emission scenarios SSP-5 with a target radioactive level of 8.5 W/m² by the end of the century [18]. The CMIP6 projections are more accurate than the CMIP5 projections in terms of temperature and precipitation uncertainties [19].

2. Methodology

2.1 Selection of Suitable GCM Based on Advanced Envelope Method

To identify the most suitable GCMs for the BGRB, this study employed the advanced envelope-based method, following the approach outlined by Lutz et al. [20]. The three steps are followed in this method as in Figure 2. The first step of the selection process involved projecting the range of annual mean temperature and total precipitation sum. In the second step, the Expert Team on Climate Change Detection and Indices (ETCCDI) was used to measure changes in daily average precipitation and temperature climate extremes. It is possible to calculate the ETCCDI indices for the historical or reference period and future periods using the online version of (https://climpact-sci-org) which uses the R-Studio interface for the calculation. After that, a final selection was made based on model performance to

simulate historical records. The projected future temperature changes can vary significantly, potentially resulting in scenarios ranging from warmer to colder condition and from wetter to drier climates. As such, GCMs are classified to reflect the full spectrum's Warm-Wet (W-W), Warm-Dry (W-D), Cold-Dry (C-D), and Cold-Wet (C-W) corners. The following flowchart illustrates the procedures used in this investigation to choose the representative climate model for any basin.

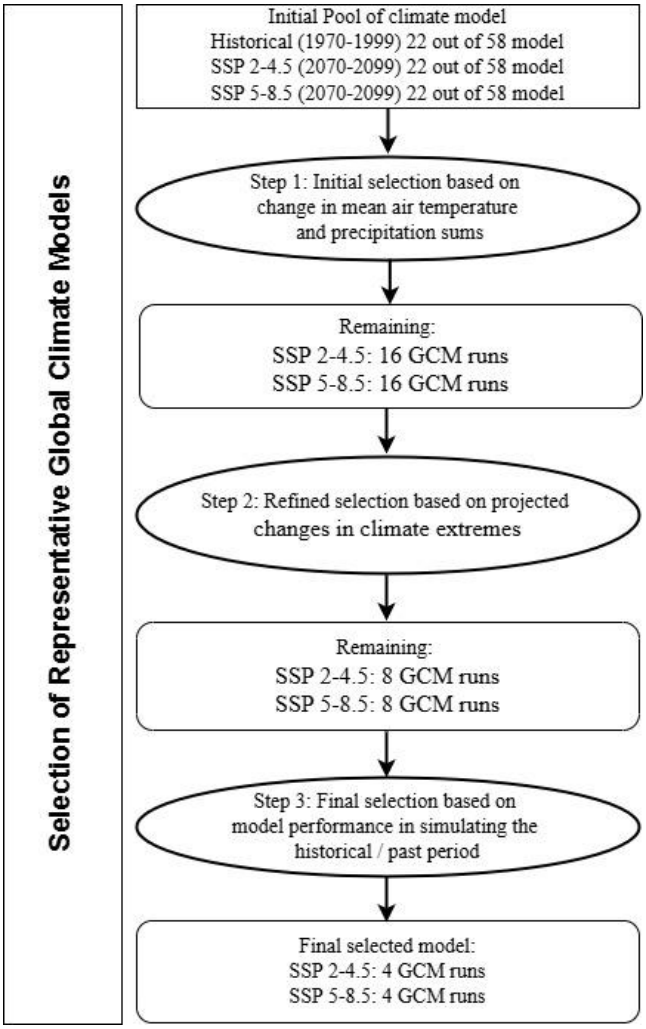

Figure 2: Flowchart illustrating the methods adopted in this study to choose the representative climate model

2.1 Initial Selection: Changes in Mean Air Temperature and Annual Precipitation Sum

We select the model that has all values of precipitation and temperature in daily time step available for Historical, SSP2-4.5, and SSP5-8.5 are the representative GCMs for BGRB out of 58 models available on the CMIP6 archive (https://cds.climate.copernicus.eu-cmip6) the data sets are available in 22 models and these model are selected for further analysis as shown in supplementary Table-3. For the study area, the annual average precipitation and mean air temperature were computed for each year of the baseline period (1970–1999) and for the future period (2070–2099), which was projected for the end of the century. Initially, 16 GCMs were selected as representative models for BGRB, with four models for each of the four climate projection corners: W-W, W-D, C-D, and C-W. The predicted range of

temperature and precipitation changes was captured by these corners. The 10th and 90th percentile values of the GCMs' average annual total precipitation (ΔP) and average annual mean air temperature (ΔT) are calculated, considering the SSP2-4.5 and SSP5-8.5 scenarios. Instead of using the minimum and maximum predictions, the 10th and 90th percentile values are employed to avoid selecting outliers [21]. The four corners W-W, W-D, C-W, and C-W represent the four extremes climate, which are 10^{th} and / or 90^{th} percentile values of ΔP and ΔT, respectively as in Table 1.

Table 1: Seasonal Forecasting for Four Extreme Climate Corners

ΔT(°C)	ΔP %	Projection
90th	90th	Warm -Wet(W-W)
90th	10th	Warm-Dry (W-D)
10th	10th	Cold-Dry (C-D)
10th	90th	Cold-Wet (C-W)

A skilled model is represented by the models that are closest to a particular corner of the spectrum in each Quartile. The distance of each model to the nearest corner of the projected climate change spectrum is calculated using a formula derived from Lutz et al. [20]. This approach ensures the selection of GCMs that span the full range of projected climate variability, specifically in terms of mean annual temperature (ΔT) and precipitation (ΔP) changes. The method involves calculating the Euclidean distance from each GCM's projected climate change signal to the four climate corner points. The proximity of the model runs percentile rank scores to each corner concerning their projections for **(**ΔP) and (ΔT) for entire GCMs was calculated using Equation 1 to calculate each model's distance (D) to the closest corner of the spectrum. The distance (D) of each model j to a specific climate corner i (e.g., warm-wet, warm-dry, cold-dry, cold-wet) is calculated using the following Euclidean distance formula:

$$D_{P_j{}^T, P_j{}^P} = \sqrt{\left(P_i^T - P_j^T\right)^2 + \left(P_i^P - P_j^P\right)^2} \quad (1)$$

Where, $D_{P_j{}^T, P_j{}^P}$ is the distance of model (j)'s ΔT and ΔP (P_j^T and P_j^P respectively) to the corner (i)'s 10^{th} and 90^{th} percentile score of ΔT and ΔP for the entire ensemble (P_j^T and P_j^P respectively). P_j^T and P_j^P are the percentile rank values of model j for ΔT and ΔP respectively.

The four models for each corner are chosen based on their lowest D values and the data that is available at each daily time step. The model with the lowest Euclidean distance (D) is considered the most representative of that extreme scenario and is consequently selected for further analysis.

2.2 Selection Based on Variations in Extreme Weather Conditions

The second step of refined selection involves further refining the subset of model runs that were kept from the first selection process. From the set of 27 indices, we focused only on a

handful of the most important extreme temperature and precipitation indications as by Sillmann et al.[22]. We analyze changes in the warm spell duration index (WSDI) and cold spell duration index (CSDI) to characterize variations in air temperature extremes. Both the precipitation resulting from exceptionally wet days (R99pTOT) and the number of consecutive dry days (CDD) are considered when characterizing changes in precipitation extremes. The indices are calculated for each of the individual stations that comprise the research region using the daily model output for each year in the reference period (1970–1999) and the future period (2070–2099). Subsequently, the indices' alterations are conveyed as a percentage change for the forthcoming period concerning the reference period. The indices are then averaged over the grid cells that encompass the research area. The Indices may be calculated from the (https://climpact-sci.org) online version for the reference period as well as future periods. The two climate extremes for temperature and precipitation considered in this study are presented in
Table 2 , using both the GCM and reference datasets.

Table 2: Explanation of ETCCDI indices used for the study

Meteorological Variable	ETCCDI Index	Description of the ETCCDI Index
Precipitation	R99PTOT	Precipitation due to extremely wet days (annual total precipitation when daily rainfall > 99th percentile)
	CDD	Consecutive dry days: maximum length of a dry spell when (precipitation <1mm)
Temperature	WSDI	Warm spell duration index: count of days in at least 6 days where maximum temperature (TX)> 90th percentile
	CSDI	Cold spell duration index: Count of days in at least 6 days where minimum temperature (TN)<10th percentile

During the refined selection process, skill scores are calculated using the most relevant temperature and precipitation index for either end of the spectrum. For example, CDD and CSDI, the models chosen for the C-D corner, are taken into consideration, whereas WSDI and CDD are considered for the warm-dry corner. Similarly, as indicated in Table 3, the models chosen from the W-W corner were assessed using the indices WSDI and R99PTOT, whereas the models chosen from the cold-wet corner were assessed using CSDI and R99PTOT. Based on the percentage increase of pertinent indices, the model ensembles were scored (T-index rank and P-index rank) by Lutz et al. [20]. In each of the four future climate corners, models are ranked from 1 to 4, with the model with the highest increase in the R99pTOT index receiving the highest rank (for example, in the W-W corner, the model with the largest increase in R99pTOT receives four points, while the model with the smallest increase receives one point). Also, the model with the largest WSDI rise receives four points for that index, while the model with the least WSDI increase receives one point. To get the final score, the two scores are then averaged. In this step, the initial selection based on mean changes is further refined by incorporating available data on climate extremes.

Table 3: ETCCDI indices lead the selection based on extremes

Projection	ETCCDI indices leading selection
Warm-Wet	WSDI and R99pTOT
Warm-Dry	WSDI and CDD
Cold-Dry	CSDI and CDD
Cold-Wet	CSDI and R99pTOT

2.3 Final Selection Based on Model Performance to Represent the Historical Climate

The models selected from the refined selection step were then assessed for their ability to reproduce the annual cycle of precipitation and air temperature data for the base period (1990–2014). The model runs were verified for their ability to replicate historical climate using monthly average data on precipitation and air temperature. The reference climate dataset was taken from the DHM. The winter bias, monsoon bias, and total bias were considered for air temperature. The biases show how different the GCMs run for the same period are from the reference value. The bias between the GCM run and the past dataset for the precipitation sum is computed annually and for the summer monsoon season (June-September). Since the monsoon season in Nepal accounts for more of all precipitation, biases originating during this time of year will be disproportionately strong. The monsoon has a significant impact on precipitation in the BGRB. For, precipitation sum the bias between the GCM run and Precipitation during the monsoon season is also essential for reservoir-based projects. Therefore, biases for temperature and precipitation between the reference data and the GCM data were calculated using the winter bias, monsoon bias, and total (annual) bias. The bias for each model in terms of temperature (T-bias) and precipitation (P-bias) are computed relative to the reference data for the historical period (e.g., 1990–2014). The temperature biases are expressed in (°C), and the precipitation biases are expressed as a (ΔP%). The maximum absolute bias is found for each climatic variable and scenario for all models taken into consideration for that variable in that scenario. The maximum (T-bias) and (P-bias) are determined by scanning through the entire ensemble of models. The bias values (P-bias and T-bias) were then determined for each scenario, SSP2-4.5, and SSP5-8.5, to normalize each absolute bias value as a percentage of the maximum absolute bias value within the model ensembles by using the equation (2) and (3) for precipitation and temperature respectively.

$$P - bias_{norm,j} = \frac{|T-bias_j|}{Max(|T-bias_j|)} \quad (2)$$

$$T - bias_{norm,j} = \frac{|P-bias_j|}{Max(|P-bias_j|)} \quad (3)$$

The normalized temperature and precipitation bias scores are averaged and added to compute the total bias score for each model. At every corner, the model with the lowest cumulative

score shows the least variation in reference values and GCM runs for the base period was selected. By ensuring that bias scores are scaled between 0 and 1 according to the highest observed absolute bias across all models, this normalization makes it possible to compare models and scenarios fairly.

4. Results and Discussion

4.1 Climate model selection based on changes in climatic means

The first choice is based on expected changes in annual precipitation total (ΔP) and mean air temperature (ΔT) between 1970–1999 and 2070–2099, which indicates a 100-year change. In each GCM run, the distance to the 10th and 90th percentile values in the corners are calculated as described above in section 3.2. The SSP5-8.5 model pool has a significantly wider range of projections for ΔT and ΔP compared to the SSP2-4.5. The value of ΔT ranges from 1.82 to 4.7°C, and ΔP ranges from −3.35 to +27.66% for SSP2-4.5, while SSP5-8.5 ΔT ranges from 3.06 to 7.12°C and ΔP ranges from +4.55 to +40.68% in the far future period 2070-2099 respectively as shown in Table 4 and Figure 3.

Table 4: GCM runs analyzed during the initial selection step based on change in annual precipitation sum (ΔP) and mean air temperature (ΔT) for each model with reference period.

Model Name	SSP2-4.5		SSP5-8.5	
	ΔP (%)	ΔT (°C)	ΔP (%)	ΔT (°C)
ACCESS-CM2 (Australia)	17.85	3.60	35.08	5.59
BCC-CSM2-MR (China)	7.85	3.15	19.08	4.88
CMCC-ESM2 (Italy)	27.66	3.78	39.75	5.90
HadGEM3-GC31-LL (UK)	10.73	2.68	27.51	4.91
IITM-ESM (India)	7.74	1.82	27.35	3.06
INM-CM5-0 (Russia)	13.94	2.24	19.82	3.66
IPSL-CM6A-LR (France)	12.27	3.98	38.97	7.07
MIROC6 (Japan)	2.04	3.10	14.81	4.69
MIROC-ES2L (Japan)	-1.13	2.38	4.55	3.89
MRI-ESM2-0 (Japan)	12.00	3.22	25.36	5.34
NorESM2-MM (Norway)	3.58	3.04	15.94	4.88
CESM2 (USA)	-3.35	3.41	8.56	5.82
CMCC-CM2-SR5 (Italy)	24.27	4.70	40.42	5.71
CNRM-CM6-1 (France)	4.19	4.43	25.50	7.12
CNRM-ESM2-1 (France)	15.98	3.72	28.90	5.98
EC-Earth3-CC (Europe)	17.55	3.18	40.68	5.68
GFDL-ESM4 (USA)	5.55	2.97	5.00	4.52
INM-CM4-8 (Russia)	15.62	2.13	26.10	3.56
KACE-1-0-G (South Korea)	14.64	3.82	34.06	6.05
MPI-ESM1-2-LR (Germany)	0.08	2.92	5.64	4.63
NESM3 (China)	5.76	3.44	10.44	5.90
UKESM1-0-LL	5.25	3.07	25.93	5.24
10th Percentile	0.28	2.25	5.93	3.69
90th Percentile	17.39	3.97	39.67	6.04

In the first step, the 10th and 90th percentile values for ΔT and ΔP in SSP2-4.5 and SSP5-8.5 scenarios, as shown in Figure 3, define the four extreme corners of the temperature and

precipitation change projection spectrum: "W-W," "W-D," "C-D," and "C-W." For each scenario, four models with daily outputs closest to these corners were selected.

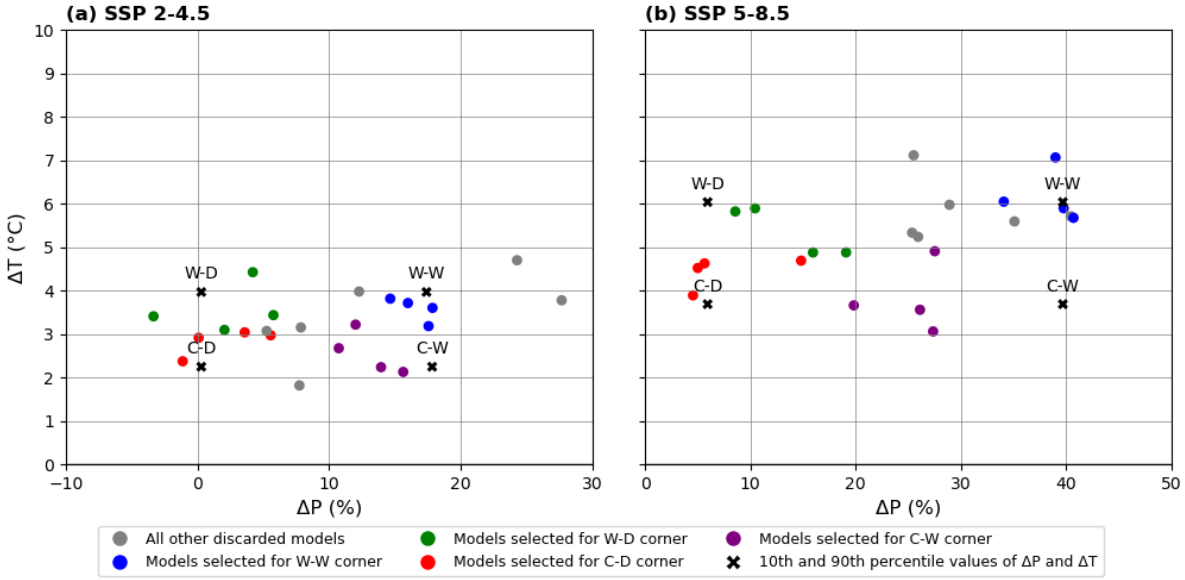

Figure 3: Projected variations in mean temperature (ΔT) and annual rainfall sum (ΔP) between the base period 1970-1999 and far future 2070-2099 for all r1i1p1f1 members of GCM (a) SSP 2-4.5 and (b) SSP 5-8.5. A black cross of larger size represents the 10th and 90th percentile values for precipitation and temperature. The rejected models from this step are indicated as grey circles. The selected models for warm-wet, warm-dry, cold-dry, and, cold-wet conditions are highlighted in blue, green, red, and purple, respectively.

The models selected in step two are highlighted in blue, green, red, and purple colours indicating the selected GCMs for the W-W, W-D, C-D, and C-W corners respectively. The black cross at each corner indicates the 10^{th} and 90^{th} percentile values for temperature (ΔT) and annual precipitation sum (ΔP). The models that are chosen for each of the four extreme corners are shown in Figure 3. There are sixteen models altogether for each scenario and research period, and we select four models that are closest to each corner of the spectrum and have daily temperature and precipitation data accessible in time series for both the past and the future.

4.2 Selection is based on variations in extreme weather conditions

Two extreme climatic indices for temperature and precipitation at the end of the century are used to assess the remaining models in the first stage relative to the reference dataset. The ETCCDI extreme indices, the T index rank, the P index rank, and the total score for all GCMs are shown in Figure 4 for both future and past periods for SSP2-4.5 and SSP5-8.5 respectively. The value with green colour indicates the selected model for each corner in this step. For the C-D corner, for instance, CDD and CSDI are used. Likewise, WSDI and CDD for the warm and dry corners, and CSDI and R99pTOT for the cold and wet corners. WSDI and R99pTOT both reflect the warm and wet corners similarly. GCM runs with the highest value in one index may not be chosen if they show the least change in another index if a consolidated score is calculated by ranking the values of the ETCCDI index. Such as the

GFDL-ESM4 (USA) model, which projects the largest changes in CSDI, is not chosen in the C-D corner when considering the future period for SSP2-4.5. KACE-1-0-G (South Korea) is not selected from the W-W corner, even though it predicts the biggest changes in R99PTOT. The C-D corner of the SSP5-8.5 MIROC-ES2L (Japan) model predicts greater changes in CSDI over the future but was not selected. Notably, although INM-CM4-8 (Russia) under SSP5-8.5 and in the C-W corner projects a substantial change in R99PTOT, it was not selected. This underscores the point that the model exhibiting the largest or smallest changes in mean temperature or precipitation may also present the most significant shifts in the corresponding extreme indices. For instance, CMCC-ESM2 (Italy) considering SSP2-4.5 predicted the highest amount of change in ΔP (+27.66%) in the future period W-W corner, which also predicted the highest increase in WSDI (1129.78%). In the far future, the number of consecutive dry days (CDD) is projected to change within a range of -16.62 to + 39.48% under SSP2-4.5, and -26.09 to + 36.56 % under SSP5-8.5, respectively. The majority of models predict that CDD will rise by up for both scenarios. The models predict that R99pTOT will rise for SSP2-4.5 and SSP5-8.5, with increases ranging from -9.03% to +40.19% and -76.37% to +5.36%, respectively. A rise in both CDD and R99pTOT suggests that the upcoming monsoon season will see more intense precipitation events.

Furthermore, by the end of the century, WSDI is expected to rise in all scenarios and eras. WSDI is predicted to increase by 201.13% to 1129.78% for SSP2-4.5 and by 248.88% to 2074.16% for SSP5-8.5. This implies that maximum temperatures in the future will probably be higher than those during the baseline period. Furthermore, the anticipated rise in WSDI draws attention to the possible consequences of growing greenhouse gas emissions and anthropogenic activity. The management of water resources, natural ecosystems, and human health may all be significantly impacted by these increases in temperature and precipitation extremes. The WSDI is expected to increase in all scenarios and time periods. The predicted CSDI changes for SSP2-4.5 and SSP5-8.5 by the end of the century varied from -87.75% to -6.4% and from -100% to -72.32%, respectively, across all models. In their respective study areas, [23], [24] also noted an increasing trend in four climatic indices, and they reported similar trends in extreme temperature and precipitation indices.

Scenario	Projection	Models	ΔWSDI (%)	ΔCDD (%)	ΔCSDI (%)	ΔR99P (%)	ΔP (%)	ΔT (°C)	T index Rank	P index Rank	Combined Score
SSP2-4.5	W-W	**CMCC-ESM2 (Italy)**	1129.78	-2.44	-85.84	17.88	27.66	3.78	4	3	**3.5**
		CNRM-ESM2-1 (France)	413.95	18.05	-82.52	-0.63	15.98	3.72	1	1	1
		IPSL-CM6A-LR (France)	414.66	1.51	-80.70	5.31	12.27	3.18	2	2	2
		EC-Earth3-CC (Europe)	442.07	-3.35	-74.69	40.19	17.55	3.18	3	4	**3.5**
	W-D	**CNRM-CM6-1 (France)**	553.01	8.28	-87.57	-5.79	4.19	4.43	3	3	**3**
		NESM3 (China)	661.24	-0.76	-72.29	-1.86	5.76	3.44	4	1	**2.5**
		MIROC6 (Japan)	297.79	39.48	-12.86	20.72	2.04	3.10	1	4	**2.5**
		IPSL-CM6A-LR (France)	414.66	1.51	-80.70	5.31	12.27	3.98	2	2	2
	C-D	**MIROC-ES2L (Japan)**	413.78	-3.86	-47.98	7.43	-1.13	2.38	4	1	**2.5**
		MPI-ESM1-2-LR (Germany)	228.41	16.72	-72.32	-7.50	0.08	2.92	2	3	**2.5**
		NorESM2-MM (Norway)	381.53	19.50	-67.01	11.92	3.58	3.04	3	4	**3.5**
		GFDL-ESM4 (USA)	308.17	1.93	-87.75	-9.03	5.55	2.97	1	2	1.5
	C-W	INM-CM4-8 (Russia)	201.13	-16.62	-65.09	-1.16	15.62	2.13	3	2	2.5
		INM-CM5-0 (Russia)	225.48	-6.73	-6.41	-6.49	13.94	2.24	2	1	1.5
		EC-Earth3-CC (Europe)	442.07	-3.35	-74.69	40.19	17.55	3.18	3	4	**3.5**
		MRI-ESM2-0 (Japan)	414.80	3.63	-87.50	22.16	12.00	3.22	4	3	**3.5**
SSP5-8.5	W-W	**IPSL-CM6A-LR (France)**	950.15	4.59	-100.00	-63.48	38.97	7.07	3	3	**3**
		CMCC-ESM2 (Italy)	1521.63	-5.03	-100.00	-64.98	39.75	5.90	4	2	**3**
		KACE-1-0-G (South Korea)	248.88	-22.19	-100.00	-67.50	34.06	6.05	1	1	1
		EC-Earth3-CC (Europe)	939.21	27.51	-100.00	-57.00	40.68	5.68	2	4	**3**
	W-D	**NESM3 (China)**	2074.16	9.77	-96.79	5.36	10.44	5.90	4	3	**3.5**
		CNRM-CM6-1 (France)	1153.01	8.38	-100.00	-74.52	25.50	7.12	3	2	**2.5**
		MRI-ESM2-0 (Japan)	543.02	29.25	-100.00	-66.61	25.36	5.34	1	4	**2.5**
		NorESM2-MM (Norway)	889.17	-26.09	-100.00	-73.13	15.94	4.88	2	1	1.5
	C-D	**GFDL-ESM4 (USA)**	877.04	36.56	-91.55	-67.96	5.00	4.52	4	3	**3.5**
		MIROC-ES2L (Japan)	548.82	10.70	-94.76	-69.09	4.55	3.89	1	1	1
		MPI-ESM1-2-LR (Germany)	376.32	24.02	-72.32	-76.37	5.64	4.63	2	4	**3**
		MIROC6 (Japan)	511.99	34.02	-92.50	-66.50	14.81	4.69	3	2	2.5
	C-W	INM-CM4-8 (Russia)	527.48	-8.11	-98.35	-74.30	26.10	3.56	2	1	1.5
		INM-CM5-0 (Russia)	387.53	-12.85	-93.59	-65.57	19.82	3.66	3	4	**3.5**
		MRI-ESM2-0 (Japan)	543.02	29.25	-100.00	-66.61	25.36	5.34	1	2	1.5
		MIROC6 (Japan)	511.99	34.02	-92.50	-66.50	4.55	3.89	4	3	**3.5**

Figure 4: GCM runs selected during the refined step which is selected for step 3 are indicated with green color having the highest combined score.

4.3 Final selection based on the model's past performance

The model runs were confirmed to accurately replicate historical climates using monthly average air temperature and precipitation data. The ability of the selected model from the narrowed selection to replicate with historical reference precipitation and air temperature data for the base period (1990–2014) was next evaluated. Biases during the monsoon, winter, and annual periods were considered for air temperature.

As previously mentioned, these biases show how much the GCM runs for the same period differs from the reference values. Finally, the models with the lowest cumulative bias score a measure of the GCM's effectiveness relative to the reference data are selected. To represent

the possible future climatic prediction of BGRB, we must select a limited group of climate models with suitable performance, using the previously discussed multi-criteria technique for selecting effective climate models. Based on the total bias of precipitation and temperature for the W-W, W-D, C-D, and C-W corners, EC-Earth3-CC, MIROC6, MPI-ESM1-2-LR, and MRI-ESM2-0 exhibit the smallest total bias values under SSP2-4.5 during the end of the century, demonstrating their high performance in simulating historical climates. Similarly, IPSL-CM6A-LR, MRI-ESM2-0, GFDL-ESM4, and INM-CM5-0 perform well for the end-of-century climate simulations under SSP5-8.5 and are shown in Table 5. In total, eight number of the best GCM models are selected to forecast the BGRB future temperature and precipitation patterns. To summarize, the representation of complex physical processes, initial and boundary data uncertainties, regional heterogeneity, coarse spatial resolution, and structural limitations are the main causes of biases in climate models. Resolving these biases requires downscaling strategies, model ensembles, and bias correction techniques in addition to ongoing advancements in model physics and resolution.

Table 5: Biases between GCM runs (2070-2099) and reference climate data set (1990-2014) for BGRB

Scenario	Projection	Model	Annual Pr	Monsoon Pr	P bias total (%)	Pbiasmon (%)	Tavg	T mon	T win	T bias total(°C)	T bias Moon(°C)	T bias win(°C)	P bias tot nor	P bias mon nor	T bias tot nor	T bias mon nor	T bias win nor	P bias score	T bias score	Total Bias
SSP2-4.5	W-W	CMCC-ESM2 (Italy)	3281.27	1626.57	104.14	40.80	11.44	14.54	7.31	-7.40	-8.99	-5.67	1.00	0.43	0.64	0.58	0.38	0.71	0.56	1.27
		EC-Earth3-CC (Europe)	2027.47	1656.07	26.14	43.36	13.97	20.10	6.16	-4.86	-3.43	-6.83	0.25	0.45	0.42	0.22	0.46	0.35	0.38	0.73
	W-D	CNRM-CM6-1 (France)	1516.07	1063.53	-5.68	7.93	7.29	14.56	-1.81	-11.54	-8.96	-14.79	-0.05	0.08	1.00	0.57	1.00	0.01	0.89	0.91
		NESM3 (China)	2221.36	1748.11	38.20	51.33	9.38	16.16	0.47	-9.46	-7.37	-12.51	0.37	0.54	0.82	0.47	0.85	0.45	0.74	1.19
		MIROC6 (Japan)	2340.13	1981.49	45.59	71.53	14.96	23.53	4.87	-3.87	0.00	-8.12	0.44	0.75	0.34	0.00	0.55	0.59	0.30	0.90
	C-D	MIROC-ES2L (Japan)	1964.84	1572.50	22.24	36.12	20.15	23.15	13.28	1.31	-0.38	0.30	0.21	0.38	0.11	0.02	0.02	0.30	0.07	0.36
		MPI-ESM1-2-LR (Germany)	1947.45	1480.60	21.16	28.17	19.47	20.75	11.48	0.63	-2.78	-1.51	0.20	0.29	0.05	0.18	0.10	0.25	0.10	0.35
		NorESM2-MM (Norway)	1934.64	51.28	20.36	95.56	13.64	7.92	18.64	-5.19	-15.61	5.66	0.20	1.00	0.45	1.00	0.38	0.60	0.57	1.17
	C-W	EC-Earth3-CC (Europe)	2027.47	1656.07	26.14	43.36	13.97	20.10	6.16	-4.86	-3.43	-6.83	0.25	0.45	0.42	0.22	0.46	0.35	0.38	0.73
		MRI-ESM2-0 (Japan)	1359.58	1065.74	-15.41	7.74	13.69	20.38	4.99	-5.15	-3.14	-7.99	-0.15	0.08	0.45	0.20	0.54	-0.03	0.41	0.37
SSP5-8.5	W-W	IPSL-CM6A-LR (France)	1882.42	1536.40	17.11	33.00	19.86	25.51	11.87	1.02	1.99	-1.11	0.14	0.37	0.12	0.24	0.10	0.25	0.14	0.40
		CMCC-ESM2 (Italy)	3591.07	1820.64	123.42	57.60	12.91	16.16	8.27	-5.93	-7.37	-4.71	1.00	0.64	0.67	0.90	0.41	0.82	0.66	1.48
		EC-Earth3-CC (Europe)	2427.40	2032.95	51.02	75.98	16.47	21.96	9.06	-2.37	-1.57	-3.92	0.41	0.85	0.27	0.19	0.34	0.63	0.27	0.90
	W-D	NESM3 (China)	2319.65	1828.35	44.32	58.27	11.84	18.23	3.10	-7.00	-5.30	-9.88	0.36	0.65	0.79	0.65	0.85	0.51	0.77	1.28
		CNRM-CM6-1 (France)	1826.74	1292.55	13.65	11.89	9.99	16.57	1.38	-8.85	-6.96	-11.60	0.11	0.13	1.00	0.85	1.00	0.12	0.96	1.08
		MRI-ESM2-0 (Japan)	1521.95	1255.30	-5.31	8.67	15.81	22.04	7.68	-3.03	-1.49	-5.31	-0.04	0.10	0.34	0.18	0.46	0.03	0.33	0.36
	C-D	GFDL-ESM4 (USA)	1806.73	1092.14	12.41	-5.46	12.85	15.35	8.85	-5.98	-8.18	-4.13	0.10	-0.06	0.68	1.00	0.36	0.02	0.68	0.70
		MPI-ESM1-2-LR (Germany)	2057.23	1689.28	27.99	46.23	10.18	16.14	2.50	-8.66	-7.38	-10.49	0.23	0.52	0.98	0.90	0.90	0.37	0.94	1.31
	C-W	INM-CM5-0 (Russia)	1951.62	855.01	21.42	-25.99	18.69	20.07	17.14	-0.14	-3.46	4.15	0.17	-0.29	0.02	0.42	0.36	-0.06	0.20	0.14
		MIROC6 (Japan)	2749.67	2188.67	71.07	89.46	15.46	20.25	7.14	-3.38	-3.28	-5.84	0.58	1.00	0.38	0.40	0.50	0.79	0.42	1.20

4.4 Uncertainty quantification and model selection

The model selection process is based on a combined bias score and model performance in reproducing historical climate data. The findings reveal that while the mean projections indicate certain trends (e.g., temperature increase, changes in precipitation), the range of projections reflects inherent uncertainties. The advanced envelope method is frequently used to evaluate the accuracy of climate projections for various extreme conditions. By combining the results of several climate models, this method increases the accuracy of future climate projections by taking into consideration a wider variety of possible outcomes. A wide spread in changes indicates higher uncertainty and should be interpreted with caution, whereas a narrow spread and strong inter-model agreement indicate greater confidence in the predicted climatic trends. These envelope methods provide crucial insights into uncertainty levels and greatly increase the accuracy of climate projections.

Table 1: Final selected model of GCM runs with projected changes in mean air temperature, precipitation, and ETCCDI indices, between 1970-1999 and 2070-2099 averaged over the study area.

SSPs	Projection	GCMs	ΔP (%)	ΔT (°C)	ΔWSDI (%)	ΔCDD (%)	ΔCSDI (%)	ΔR99P (%)
SSP2-4.5	Warm-Wet	EC-Earth3-CC (Europe)	17.55	3.18	442.07	-3.35	-74.69	40.19
	Warm-Dry	MROC6 (Japan)	2.04	3.10	297.79	39.48	-12.86	20.72
	Cold-Dry	MPI-ESMI-2-LR (Germany)	0.08	2.92	228.41	16.72	-72.32	-7.50
	Cold-Wet	MRI-ESM2-0 (Japan)	12.00	3.22	414.80	3.63	-87.50	22.16
SSP5-8.5	Warm-Wet	IPSL-CM6A-LR (France)	38.97	7.07	950.15	4.59	-100.00	-63.48
	Warm-Dry	MRI-ESM2-0 (Japan)	25.36	5.34	543.02	29.25	-100.00	-66.61
	Cold-Dry	GFDL-ESM4 (USA)	5.00	4.52	877.04	36.56	-91.55	-67.96
	Cold-Wet	INM-CM5-0 (Russia)	19.82	3.66	387.53	-12.85	-93.59	-65.57

A comparison of the predicted climate changes over the BGRB under SSP2-4.5 (moderate emission) and SSP5-8.5 (high emission) for the far future (2070–2029) is shown in Table 1 and indicates the significant variability indicating the uncertainty in future climate projections. Several selected GCMs assesses changes in important climatic indices across four climate corners W-W, W-D, C-D, and C-W. The climate models predict significant warming (up to 7.07°C) and intensification of warm spells (ΔWSDI > 900%) under SSP5-8.5, particularly for Warm-Wet condition. A significant drop in cold spell duration (ΔCSDI) of up to -100% is anticipated, indicating significantly warmer winters. Although the changes are less pronounced under SSP2-4.5, but W-W still shows enhanced precipitation extremes and increased warming. Under SSP5-8.5, C-D conditions exhibit mixed precipitation trends, with notable decreases in extreme rainfall events (ΔR99P) but increases in warm spells and dry days.

The temperature (ΔT) varies between 2.92°C and 3.22°C under SSP2-4.5 and 3.66°C and 7.07°C under SSP5-8.5, suggesting that models predict moderate warming to more intense warming. Variations in precipitation (ΔP) range from almost zero (0.08%) to significant increases (38.97%), indicating a high degree of uncertainty regarding the evolution of

precipitation. With a wide range of divergence from 40.19% to -67.96%, ΔR99P (%), which represents extreme rainfall, indicates high model disagreement on heavy precipitation extremes. The magnitude of these changes varies significantly between models, but SSP5-8.5 typically predicts more drastic changes and stronger warming than SSP2-4.5. As an illustration of the strong scenario influence and sensitivity of extremes to emission pathways, under SSP5-8.5, the warm spell duration (ΔWSDI) increases range from 387.53% to 950.15%.

Dry spells are represented by ΔCDD and cold spells by ΔCSDI, which have opposite trends among GCMs and exhibit extreme variations. For example, ΔCDD can range from -12.85% to 39.48%, while ΔCSDI frequently reaches -100%, which in some projections indicate the complete disappearance of cold events. Due to variations in regional climate sensitivities and GCM performance across different climatic regimes, corner combinations (e.g., W-W vs. C-D) exhibit distinct climate responses even within the same scenario. For instance, under SSP245, C-D exhibits nearly no change in precipitation (0.08%) but a significant reduction in the length of the cold spell (-72.32%), whereas W-W exhibits significantly greater changes. Table 1 highlights the significance of employing advanced envelope approaches rather than depending solely on single models by illustrating the high levels of intra-scenario and inter-model variability. Due to the more intricate mechanisms controlling rainfall generation and variability, precipitation, and extremes (WSDI, R99P) projections exhibit higher levels of uncertainty than temperature projections. Under SSP5-8.5, wider spreads in ΔWSDI, ΔCDD, and ΔR99P signify greater uncertainty under higher forcing scenarios, which is crucial for risk-based planning.

The BGRB anticipated climate change impacts are consistent with findings from other studies carried out throughout Nepal and the Himalayan region, which show a consistent trend of rising temperatures and an increase in the frequency of extreme precipitation events. In the Tamakoshi basin, for example, [25] projected that temperatures would rise by about 1.1 to 1.5°C and an 8 to 16% increase in precipitation as compared to the 1961 -1990 period under different SSP scenarios. In a similar Dahal et al. [26], studied the Karnali River Basin and predicted temperature increases of 1.4 to 3.4 °C for SSP2-4.5 and 1.8 to 6.6°C for SSP5-8.5; however, their precipitation projections showed 12% and 30% for SSP2-4.5 and SSP5-8.5 scenarios. Similar to the trends found in this study, Bajracharya et al. [27] 2018) noted a maximum temperature increase of about 4°C and a 26% increase in precipitation in the Kaligandaki River Basin under SSP5-8.5 scenarios. All of these regional studies support the overall trend of warming and rising climate extremes in the river basins of Nepal and the Himalayas, highlighting the significance of basin-specific analyses such as this one for efficient planning of climate adaptation.

5. Conclusions

To choose representative GCMs from CMIP6 for predicting future climate change impacts in the BGRB, this study used an advanced envelope approach. Finding models that could replicate both the central tendencies and the extremes of regional climate was made possible by the selection process, which combined ranges of mean climate change, extreme weather variability, and model performance based on historical data. The findings show considerable uncertainties in precipitation changes, with estimates ranging from 0.08% to 38.97%, and a

significant projected temperature increase by the end of the century under SSP2-4.5 and SSP5-8.5 scenarios, ranging from 2.92°C to 7.07°C. Significantly, all of the models that were chosen predict an increase in warming periods and extreme precipitation events, highlighting the increased risk of climate-related hazards. These findings are crucial for managing hazards and adapting to climate change in mountainous areas like BGRB, where local topography makes climate variability worse. In order to give policymakers trustworthy data for planning resilient infrastructure and disaster preparedness, the model selection framework makes sure that impact assessments consider models that accurately capture regional climate dynamics. However, this method has some drawbacks, such as its dependence on GCM outputs without regional downscaling, which could improve local projections, especially for precipitation patterns influenced by complex topography. Climate modeling's inherent uncertainties also call for careful interpretation and the implementation of flexible approaches that can account for future variability. Future studies should concentrate on downscaling climate projections and using regional observational data to validate model outputs. In the end, these initiatives will support more effective climate adaptation policies in the BGRB and other vulnerable regions by improving the resolution and dependability of impact assessments.

Conflicts of Interest Statement

The authors declare no conflicts of interest for this study.

Data Availability Statement

The data that support the findings of this study are available from the corresponding author upon reasonable request.

References

1. IPCC, Summary for Policymakers. In: Climate Change 2021: The Physical Science Basis. Contribution of Working Group I to the Sixth Assessment Report of the Intergovernmental Panel on Climate Change, 2021.
2. R. Karki, S. ul Hasson, L. Gerlitz, R. Talchabhadel, U. Schickhoff, T. Scholten, and J. Böhner, "Rising mean and extreme near-surface air temperature across Nepal," *Int. J. Climatol.*, vol. 40, no. 4, pp. 2445–2463, 2020, doi: 10.1002/joc.6344.
3. Y. P. Dhital, J. Tang, A. K. Pokharel, Q. Tang, and M. Rai, "Impact of aerosol concentration on elevation-dependent warming pattern in the mountains of Nepal," *Atmos. Sci. Lett.*, vol. 23, no. 10, 2022, doi: 10.1002/asl.1101.
4. G. A. Meehl et al., "Decadal Climate Prediction: An Update from the Trenches," *Bull. Am. Meteorol. Soc.*, vol. 95, no. 2, pp. 243–267, 2014, doi: 10.1175/BAMS-D-12-00241.1.
5. H. Biemans et al., "Future water resources for food production in five South Asian river basins and potential for adaptation—A modeling study," *Sci. Total Environ.*, vol. 468–469, pp. S117–S131, 2013, doi: 10.1016/j.scitotenv.2013.05.092.
6. D. W. Pierce, T. P. Barnett, B. D. Santer, and P. J. Gleckler, "Selecting global climate models for regional climate change studies," *Proc. Natl. Acad. Sci. U.S.A.*, vol. 106, no. 21, pp. 8441–8446, 2009, doi: 10.1073/pnas.0900094106.
7. S.-K. Min, X. Zhang, F. W. Zwiers, and G. C. Hegerl, "Human contribution to more-intense precipitation extremes," *Nature*, vol. 470, no. 7334, pp. 378–381, 2011, doi: 10.1038/nature09763.

8. X. Zhang et al., "Indices for monitoring changes in extremes based on daily temperature and precipitation data," *WIREs Clim. Change*, vol. 2, no. 6, pp. 851–870, 2011, doi: 10.1002/.
9. V. V. Kharin, F. W. Zwiers, X. Zhang, and M. Wehner, "Changes in temperature and precipitation extremes in the CMIP5 ensemble," *Clim. Change*, vol. 119, no. 2, pp. 345–357, 2013, doi: 10.1007/s10584-013-0705-8.
10. D. Finger, G. Heinrich, A. Gobiet, and A. Bauder, "Projections of future water resources and their uncertainty in a glacierized catchment in the Swiss Alps and the subsequent effects on hydropower production during the 21st century," *Water Resour. Res.*, vol. 48, no. 2, 2012, doi: 10.1029/2011WR010733.
11. M. Minville, F. Brissette, and R. Leconte, "Uncertainty of the impact of climate change on the hydrology of a nordic watershed," *J. Hydrol.*, vol. 358, no. 1–2, pp. 70–83, 2008, doi: 10.1016/j.jhydrol.2008.05.033.
12. W. W. Immerzeel, F. Pellicciotti, and M. F. P. Bierkens, "Rising river flows throughout the twenty-first century in two Himalayan glacierized watersheds," *Nat. Geosci.*, vol. 6, no. 9, pp. 742–745, 2013, doi: 10.1038/ngeo1896.
13. L. Warszawski et al., "The Inter-Sectoral Impact Model Intercomparison Project (ISI–MIP): Project framework," *Proc. Natl. Acad. Sci. U.S.A.*, vol. 111, no. 9, pp. 3228–3232, 2014, doi: 10.1073/pnas.1312330110.
14. V. Ongoma, H. Chen, and C. Gao, "Evaluation of CMIP5 twentieth century rainfall simulation over the equatorial East Africa," *Theor. Appl. Climatol.*, vol. 135, no. 3–4, pp. 893–910, 2019, doi: 10.1007/s00704-018-2392-x.
15. A. F. Lutz et al., "Selecting representative climate models for climate change impact studies: an advanced envelope-based selection approach," *Int. J. Climatol.*, vol. 36, no. 12, pp. 3988–4005, 2016, doi: 10.1002/joc.4608.
16. S. Kaini, S. Nepal, S. Pradhananga, T. Gardner, and A. K. Sharma, "Representative general circulation models selection and downscaling of climate data for the transboundary Koshi river basin in China and Nepal," *Int. J. Climatol.*, vol. 40, no. 9, pp. 4131–4149, 2020, doi: 10.1002/joc.6447.
17. S. A. Salman, S. Shahid, T. Ismail, K. Ahmed, and X.-J. Wang, "Selection of climate models for projection of spatiotemporal changes in temperature of Iraq with uncertainties," *Atmos. Res.*, vol. 213, pp. 509–522, 2018, doi: 10.1016/j.atmosres.2018.07.008.
18. M. J. Gidden et al., "Global emissions pathways under different socioeconomic scenarios for use in CMIP6: a dataset of harmonized emissions trajectories through the end of the century," *Geosci. Model Dev.*, vol. 12, no. 4, pp. 1443–1475, 2019, doi: 10.5194/gmd-12-1443-2019.
19. M. M. Hamed, M. S. Nashwan, M. S. Shiru, and S. Shahid, "Comparison between CMIP5 and CMIP6 Models over MENA Region Using Historical Simulations and Future Projections," *Sustainability*, vol. 14, no. 16, p. 10375, 2022, doi: 10.3390/su141610375.
20. A. F. Lutz et al., "Selecting representative climate models for climate change impact studies: an advanced envelope-based selection approach," *Int. J. Climatol.*, vol. 36, no. 12, pp. 3988–4005, 2016, doi: 10.1002/joc.4608.
21. W. W. Immerzeel, F. Pellicciotti, and M. F. P. Bierkens, "Rising river flows throughout the twenty-first century in two Himalayan glacierized watersheds," *Nat. Geosci.*, vol. 6, no. 9, pp. 742–745, 2013, doi: 10.1038/ngeo1896.
22. J. Sillmann, V. V. Kharin, F. W. Zwiers, X. Zhang, and D. Bronaugh, "Climate extremes indices in the CMIP5 multimodel ensemble: Part 2. Future climate

projections," *J. Geophys. Res. Atmos.*, vol. 118, no. 6, pp. 2473–2493, 2013, doi: 10.1002/jgrd.50188.
23. S. H. Gebresellase, Z. Wu, H. Xu, and W. I. Muhammad, "Evaluation and selection of CMIP6 climate models in Upper Awash Basin (UBA), Ethiopia," *Theor. Appl. Climatol.*, vol. 149, no. 3–4, pp. 1521–1547, 2022, doi: 10.1007/s00704-022-04056-x.
24. H. W. Tenfie, F. Saathoff, D. Hailu, and A. Gebissa, "Selection of Representative General Circulation Models for Climate Change Study Using Advanced Envelope-Based and Past Performance Approach on Transboundary River Basin, a Case of Upper Blue Nile Basin, Ethiopia," *Sustainability*, vol. 14, no. 4, 2022, doi: 10.3390/su14042140.
25. D. Khadka and D. Pathak, "Climate change projection for the marsyangdi river basin, Nepal using statistical downscaling of GCM and its implications in geodisasters," *Geoenviron. Disasters*, vol. 3, no. 1, 2016, doi: 10.1186/s40677-016-0050-0.
26. P. Dahal, M. L. Shrestha, J. Panthi, and D. Pradhananga, "Modeling the future impacts of climate change on water availability in the Karnali River Basin of Nepal Himalaya," *Environ. Res.*, vol. 185, 2020, doi: 10.1016/j.envres.2020.109430.
27. A. R. Bajracharya, S. R. Bajracharya, A. B. Shrestha, and S. B. Maharjan, "Climate change impact assessment on the hydrological regime of the Kaligandaki Basin, Nepal," *Sci. Total Environ.*, vol. 625, pp. 837–848, 2018, doi: 10.1016/j.scitotenv.2017.12.332.

SUPPLEMENTARY MATERIAL

Table S1 Catchment area description of basin with details.

Description of the Catchment	Area of the Catchment (Km^2)
Gorkha	2700
Dhading	900
Nuwakot	35
China	1365
Total	5000

Table S2 List of meteorological observed stations used in the study.

Station Name	Lat (°N)	Long (°N)	Elevation(m)	Data Period	Data available
Jagat (Setibas)	28.37	84.90	1334	1990-2014	P
Larke (Samdo)	28.67	84.62	3650	1990-2014	P
Chhekampar	28.48	85.00	3300	1976-2005	P
Arughat Bazar	28.05	84.82	518	1976-2005	P
Dhading	27.87	84.93	1420	1976-2005	P
Thamachit	28.17	85.32	1847	1976-2005	P
Pansaya Khola	28.02	85.12	1240	1976-2005	P
Gorkha (Birenchowk)	28.00	84.62	1097	1990-2014	P,

Table S3 List of selected CMIP6 model for their study and their resolution.

Model Name	Research Centre	Country	Lat(°)	Long(°)
ACCESS-CM2	Australian Community Climate and Earth System Simulator (ACCESS)	Australia	1.25	1.87
BCC-CSM2-MR	Beijing Climate Center, Beijing	China	1.13	1.13
CMCC-ESM2	Centro Euro-Mediterraneo sui Cambiamenti Climatici	Italy	1	1
HadGEM3-GC31-LL	MOHC NERC (Met Office Hadley Centre, Natural Environmental Research Council)	United Kingdom	1.25	1.87
IITM-ESM	CCCR-IITM (Centre for Climate Change Research, Indian Institute of Tropical Meteorology)	India	1	1
INM-CM5-0	INM (Institute of Numerical Mathematics)	Russia	1.5	2
IPSL-CM6A-LR	IPSL (Institute Pierre-Simon Laplace)	France	1.25	2.5
MIROC6	MIROC (Atmosphere and Ocean Research Institute (AORI), Centre for Climate System Research - National Institute for Environmental Studies (CCSR-NIES) and Atmosphere and Ocean Research Institute (AORI))	Japan	1.41	1.41
MIROC-ES2L	MIROC (Atmosphere and Ocean Research Institute (AORI), Centre for Climate System Research - National Institute for Environmental Studies (CCSR-NIES) and Atmosphere and Ocean Research Institute (AORI))	Japan	1	1
MRI-ESM2-0	MRI (Meteorological Research Institute, Japan)	Japan	1.13	1.13
NorESM2-MM	NCC (Norwegian Climate Centre)	Norway	0.94	0.94
CESM2	NCAR (National Center for Atmospheric Research)	USA	0.94	1.25
CMCC-CM2-SR5	Fondazione Centro Euro-Mediterraneo sui Cambiamenti Climatic	Italy	0.937	1.25
CNRM-CM6-1	Centre National de Recherches Meteorologiques, Toulouse 31057, France	France	1.40	1.40
CNRM-ESM2-1	Centre National de Recherches Meteorologiques, Toulouse 31057, France	France	3	1
EC-Earth3-CC	EC-Earth-Consortium	Europe	0.70	0.70
GFDL-ESM4	NOAA-GFDL (National Oceanic and Atmospheric Administration, Geophysical Fluid Dynamics Laboratory	USA	1	1.25
INM-CM4-8	INM (Institute of Numerical Mathematics)	Russia	1.5	2
KACE-1-0-G (South Korea)	NIMS-KMA (National Institute of Meteorological Sciences/Korea Met. Administration)	South Korea	1.25	1.875
MPI-ESM1-2-LR (Germany)	MPI-M AWI (Max Planck Institute for Meteorology (MPI-M), AWI (Alfred Wegener Institute))	Germany	1.875	1.875
NESM3 (China)	NUIST (Nanjing University of Information Science and Technology)	China	1.875	1.875
UKESM1-0-LL	MOHC, NERC, NIMS-KMA, NIWA (Met Office Hadley Centre, Natural Environmental Research Council, National Institute of Meteorological Science / Korean Meteorological Administration (NIMS-KMA), National Institute of Weather and Atmospheric Research (NIWA))	United Kingdom	1	1

Table S4 Selected four model at each extreme condition for each scenario in initial step-1.

Projection	SSP2-4.5	SSP5-8.5
Warm-Wet (Q1)	CMCC-ESM2 (Italy)	IPSL-CM6A-LR (France)
	CNRM-ESM2-1 (France)	CMCC-ESM2 (Italy)
	IPSL-CM6A-LR (France)	KACE-1-0-G (South Korea)
	EC-Earth3-CC (Europe)	EC-Earth-3-CC (Europe)
Warm-Dry (Q2)	CNRM-CM6-1 (France)	NESM3 (China)
	NESM3 (China)	CNRM-CM6-1 (France)
	MIROC6 (Japan)	MRI-ESM2-0 (Japan)
	IPSL-CM6A-LR (France)	NorESM2-MM (Norway)
Cold-Dry (Q3)	MIROC-ES2L (Japan)	GFDL-ESM4 (USA)
	MPI-ESM1-2-LR (Germany)	MIROC-ES2L (Japan)
	NorESM2-MM (Norway)	MPI-ESM1-2-LR (Germany)
	GFDL-ESM4 (USA)	MIROC6 (Japan)
Cold-Wet (Q4)	INM-CM4-8 (Russia)	INM-CM4-8 (Russia)
	INM-CM5-0 (Russia)	INM-CM5-0 (Russia)
	EC-Earth3-CC (Europe)	MRI-ESM2-0 (Japan)
	MRI-ESM2-0 (Japan)	MIROC6 (Japan)

Table S5 Percentile rank scores corresponding to their projections for ΔT and ΔP concerning the entire range of projection for SSP2-4.5.

Model Name	ΔP (%)	ΔT (°C)	ΔP Rank	ΔT Rank
ACCESS-CM2 (Australia)	17.85	3.60	0.90	0.71
BCC-CSM2-MR (China)	7.85	3.15	0.48	0.48
CMCC-ESM2 (Italy)	27.66	3.78	1.00	0.81
HadGEM3-GC31-LL (UK)	10.73	2.68	0.52	0.19
IITM-ESM (India)	7.74	1.82	0.43	0.00
INM-CM5-0 (Russia)	13.94	2.24	0.67	0.10
IPSL-CM6A-LR (France)	12.27	3.98	0.62	0.90
MIROC6 (Japan)	2.04	3.10	0.14	0.43
MIROC-ES2L (Japan)	-1.13	2.38	0.05	0.14
MRI-ESM2-0 (Japan)	12.00	3.22	0.57	0.57
NorESM2-MM (Norway)	3.58	3.04	0.19	0.33
CESM2 (USA)	-3.35	3.41	0.00	0.62
CMCC-CM2-SR5 (Italy)	24.27	4.70	0.95	1.00
CNRM-CM6-1 (France)	4.19	4.43	0.24	0.95
CNRM-ESM2-1 (France)	15.98	3.72	0.81	0.76
EC-Earth3-CC (Europe)	17.55	3.18	0.86	0.52
GFDL-ESM4 (USA)	5.55	2.97	0.33	0.29
INM-CM4-8 (Russia)	15.62	2.13	0.76	0.05
KACE-1-0-G (South Korea)	14.64	3.82	0.71	0.86
MPI-ESM1-2-LR (Germany)	0.08	2.92	0.10	0.24
NESM3 (China)	5.76	3.44	0.38	0.67
UKESM1-0-LL	5.25	3.07	0.29	0.38

Table S6 Percentile rank scores corresponding to their projections for ΔT and ΔP concerning the entire range of projection for SSP5-8.5.

Model Name	ΔP (%)	ΔT (°C)	ΔP Rank	ΔT Rank
ACCESS-CM2 (Australia)	35.08	5.59	0.81	0.57
BCC-CSM2-MR (China)	19.08	4.88	0.33	0.38
CMCC-ESM2 (Italy)	39.75	5.90	0.90	0.81
HadGEM3-GC31-LL (UK)	27.51	4.91	0.67	0.43
IITM-ESM (India)	27.35	3.06	0.62	0.00
INM-CM5-0 (Russia)	19.82	3.66	0.38	0.10
IPSL-CM6A-LR (France)	38.97	7.07	0.86	0.95
MIROC6 (Japan)	14.81	4.69	0.24	0.29
MIROC-ES2L (Japan)	4.55	3.89	0.00	0.14
MRI-ESM2-0 (Japan)	25.36	5.34	0.43	0.52
NorESM2-MM (Norway)	15.94	4.88	0.29	0.33
CESM2 (USA)	8.56	5.82	0.14	0.71
CMCC-CM2-SR5 (Italy)	40.42	5.71	0.95	0.67
CNRM-CM6-1 (France)	25.50	7.12	0.48	1.00
CNRM-ESM2-1 (France)	28.90	5.98	0.71	0.86
EC-Earth3-CC (Europe)	40.68	5.68	1.00	0.62
GFDL-ESM4 (USA)	5.00	4.52	0.05	0.19
INM-CM4-8 (Russia)	26.10	3.56	0.57	0.05
KACE-1-0-G (South Korea)	34.06	6.05	0.76	0.90
MPI-ESM1-2-LR (Germany)	5.64	4.63	0.10	0.24
NESM3 (China)	10.44	5.90	0.19	0.76
UKESM1-0-LL	25.9	5.24	0.52	0.48

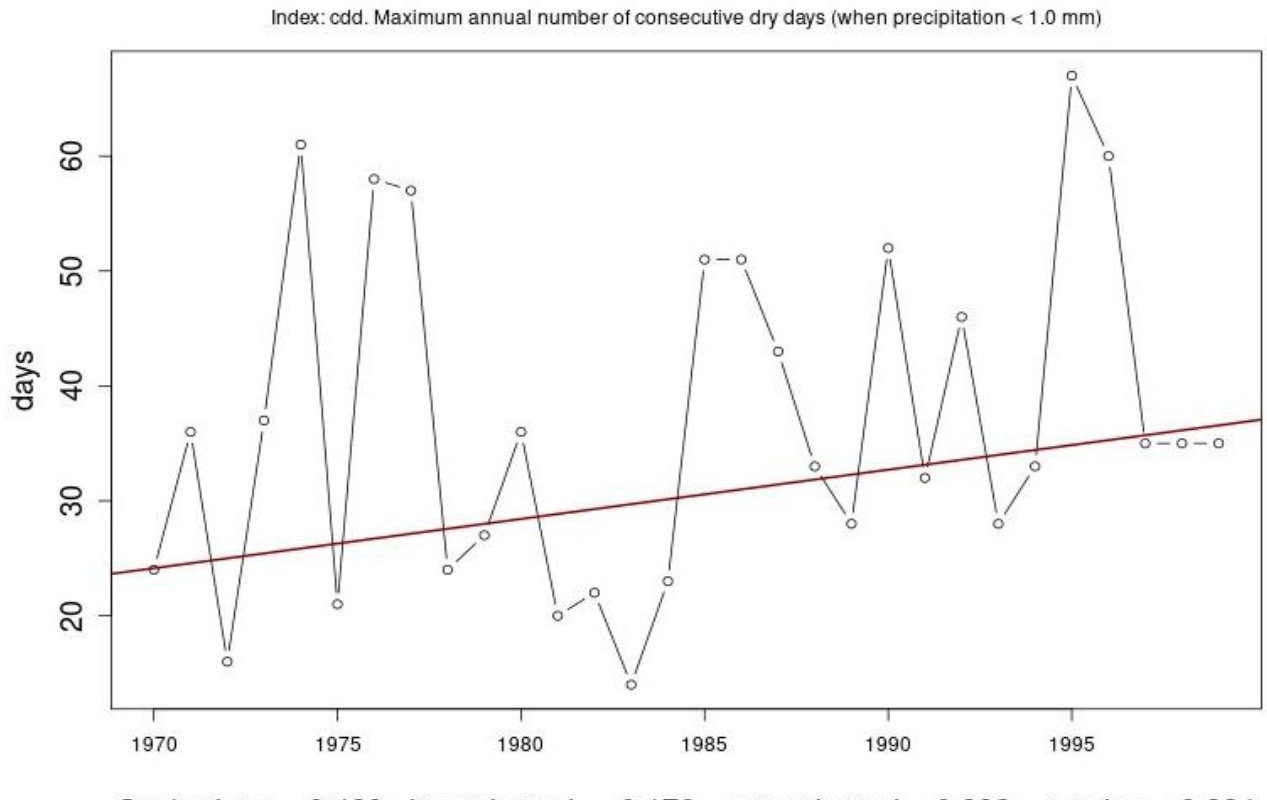

Figure S1: ***The EC-Earth3-CC (Europe) historical simulation was used to determine the temporal variation in the maximum annual number of consecutive dry days CDD between 1970 and 1999. With a marginally positive trend of 0.429 days annually, the red line represents the Sen's slope trend estimate. With a 95% confidence interval spanning from -0.176 to 0.882, the trend is statistically non-significant (p = 0.224), despite suggesting an increase in dry spells. This suggests that there has been no discernible long-term trend in extreme dry events over the historical period, but there is moderate interannual variability under*** *W-W corner in SSP2-4.5 scenario from (https://climpact-sci.org).*

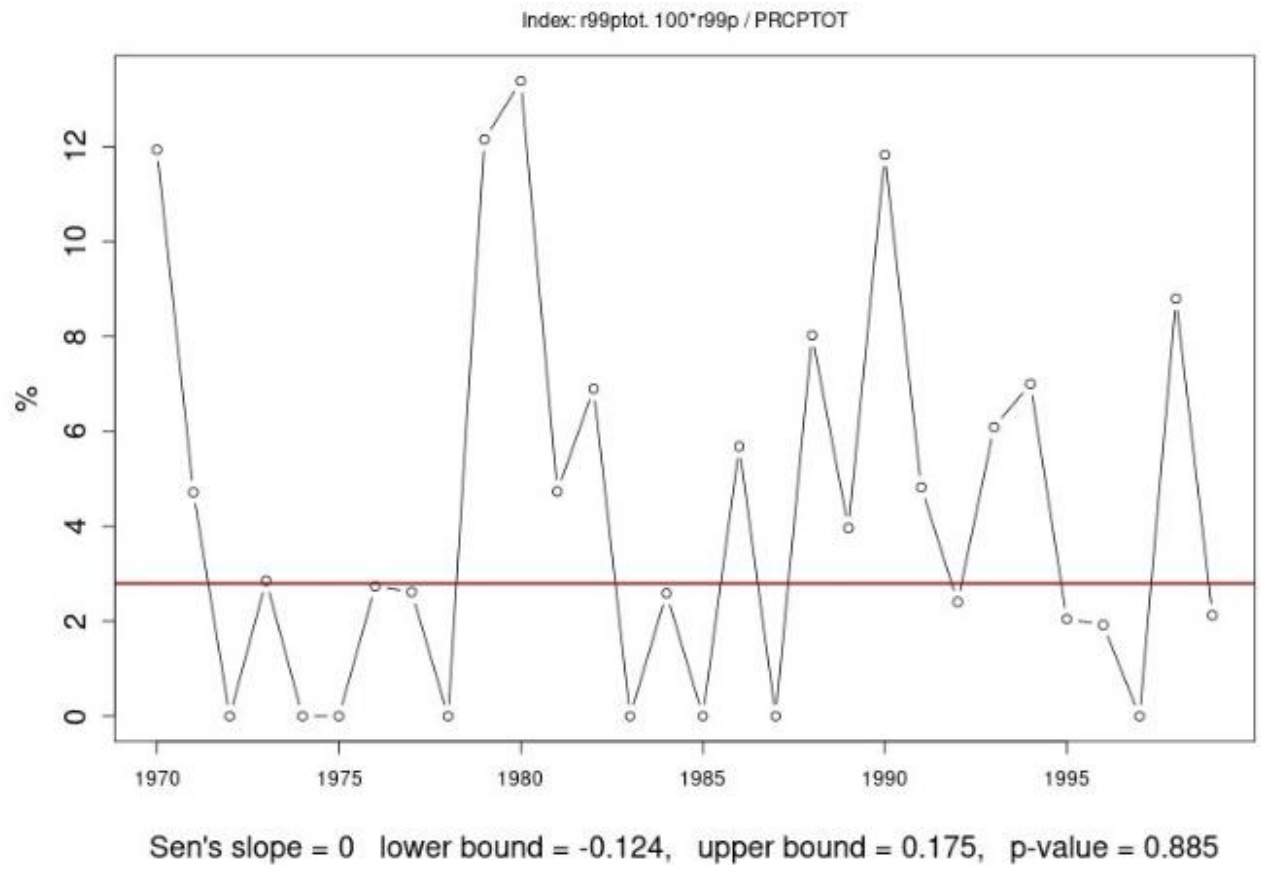

Figure S2: ***The EC-Earth3-CC (Europe) model generated a historical trend of the percentage contribution of extreme precipitation events (R99pTOT; annual total precipitation from days exceeding the 99th percentile) to total annual precipitation between 1970 and 1999. Sen's slope trend, represented by the red line, is zero, meaning there is no discernible trend over time. The trend is not statistically significant (p = 0.885). This implies that while there was no discernible rise or fall in the extreme precipitation events' share of the total precipitation over the historical period, there was a high degree of interannual variability under W-W Corner in SSP2-4.5 scenario from (https://climpact-sci.org).***

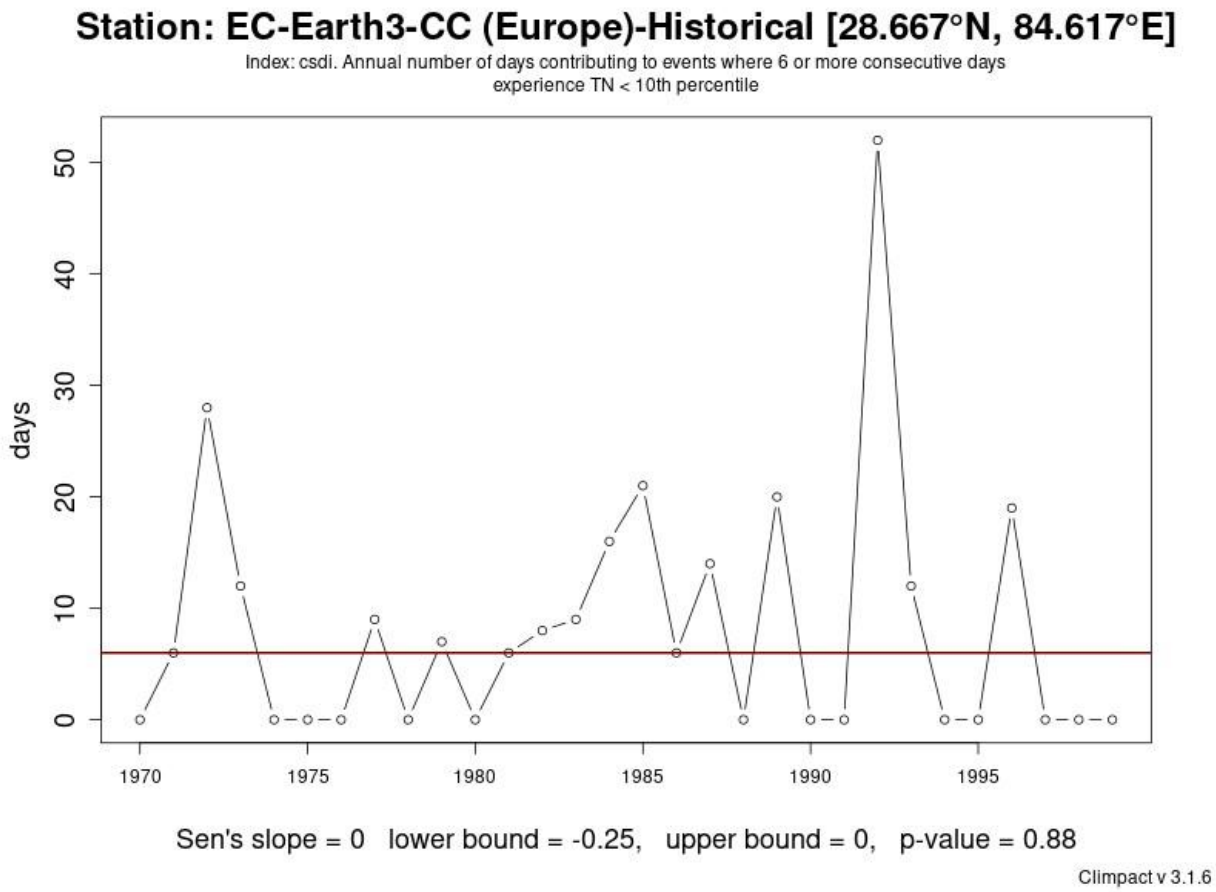

Figure S3: ***The EC-Earth3-CC (Europe) model generated a historical trend of the percentage contribution of extreme cold event (CSDI; Annual number of days contributing to events where 6 or more consecutive days not exceeding the 10th percentile) to total annual precipitation between 1970 and 1999. Sen's slope trend, represented by the red line, is zero, meaning there is no discernible trend over time. The trend is not statistically significant (p = 0.88). This implies that while there was no discernible rise or fall in the extreme precipitation events' share of the total precipitation over the historical period, there was a high degree of interannual variability under W-W Corner in SSP2-4.5 scenario from (https://climpact-sci.org).***

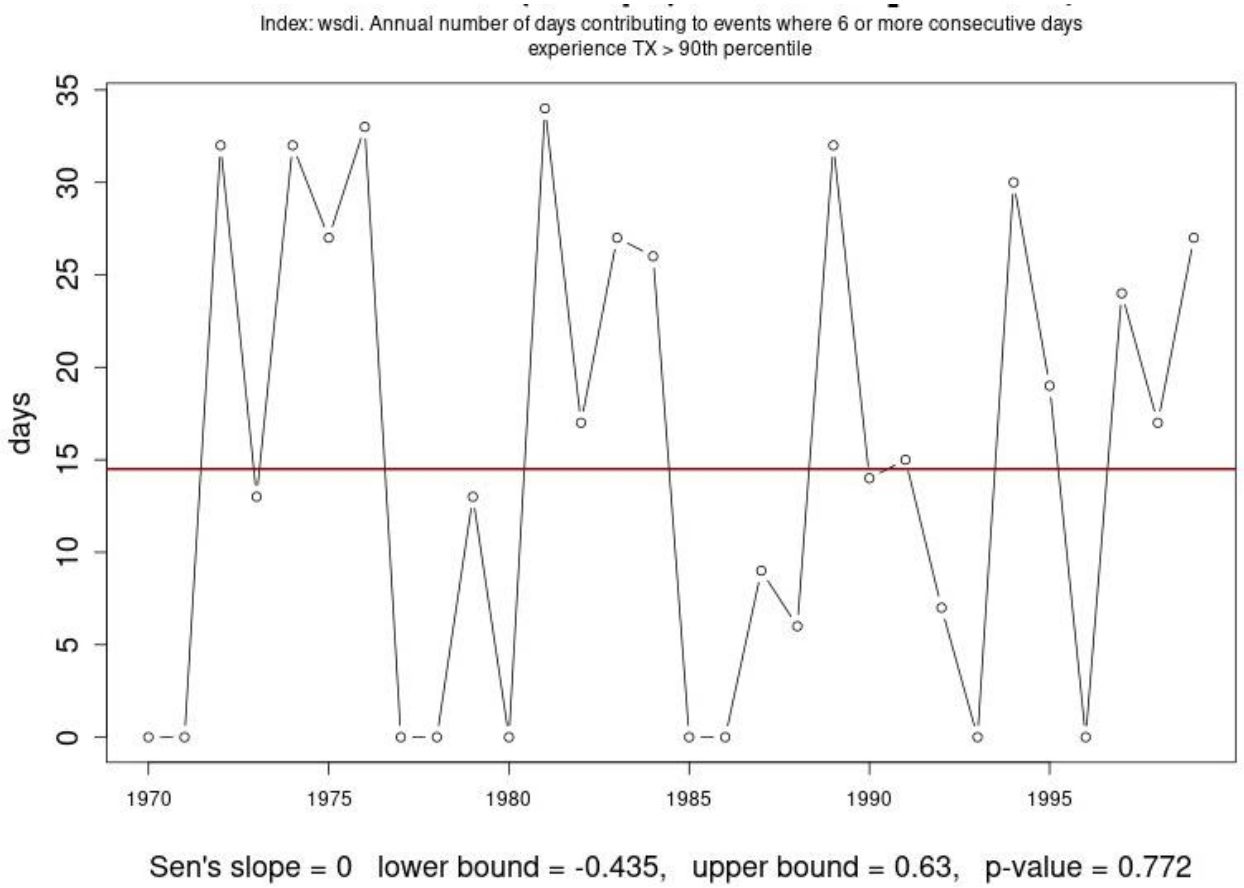

Figure S4*: The EC-Earth3-CC (Europe) model generated a historical trend of the percentage contribution of extreme warm (WSDI; Annual number of days contributing to events where 6 or more consecutive days exceeding the 90th percentile) to total annual precipitation between 1970 and 1999. Sen's slope trend, represented by the red line, is zero, meaning there is no discernible trend over time. The trend is not statistically significant (p = 0.72). This implies that while there was no discernible rise or fall in the extreme precipitation events' share of the total precipitation over the historical period, there was a high degree of interannual variability under W-W Corner in SSP2-4.5 scenario from (https://climpact-sci.org).*